Electronic Supplementary Material (ESI) for Journal of Materials Chemistry C.
This journal is © The Royal Society of Chemistry 2024

Electronic Supplementary Information†

Structured Carbon Nanotubes-Elastomer Nanocomposites with Morphing-Contact Mechanism for Advanced Underwater Perception Alarming System

Feng Deng[ab], Peng Xiao*[ab],Wei Zhou[ab] ,Qing Yang[c], Tao Chen*[ab]

[a]Key Laboratory of Marine Materials and Related Technologies, Zhejiang Key Laboratory of Marine Materials and Protective Technologies, Ningbo Institute of Materials Technology and Engineering, Chinese Academy of Sciences, Zhongguan West Road 1219, Ningbo 315201, China.

[b]School of Chemical Sciences, University of Chinese Academy of Sciences, 19A Yuquan Road, Beijing 100049, China.

[c]State Key Laboratory of Modern Optical Instrumentation, College of Optical Science and Engineering, International Research Center for Advanced Photonics, Zhejiang University, Hangzhou 310027, China

*Corresponding author: Peng Xiao (xiaopeng@nimte.ac.cn) and Tao Chen (tao.chen@nimte.ac.cn)

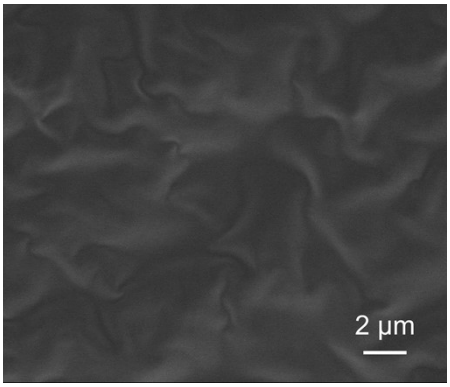

Fig. S1. SEM image of the CNTs/ Ecoflex Janus film with smooth surface morphology on Ecoflex side.

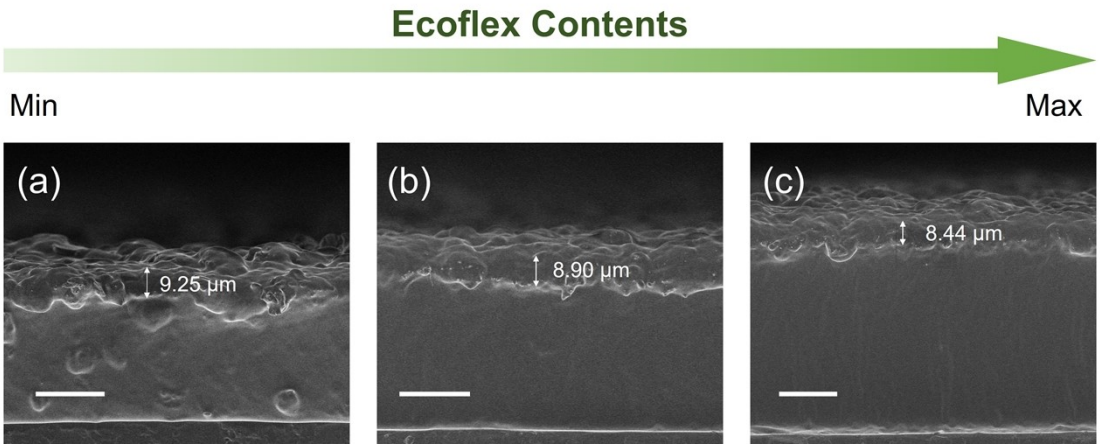

Figure S2. Cross-sectional SEM images of Janus films produced by Ecoflex additions of (a) 0.8 g:0.8 g, (b) 1 g:1 g and (c) 1.2 g:1.2 g. Bar: 20 μm.

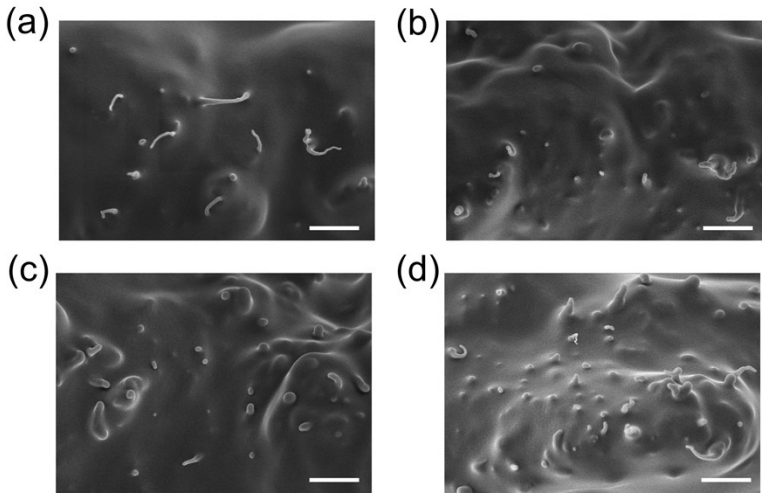

Figure S3. Surface SEM images of Janus films prepared with COOH-MWCNTs dispersions at concentrations of (a) 1.0 mg/mL, (b) 1.5 mg/mL, (c) 2.0 mg/mL and (d) 2.5 mg/mL. Bar: 2 μm.

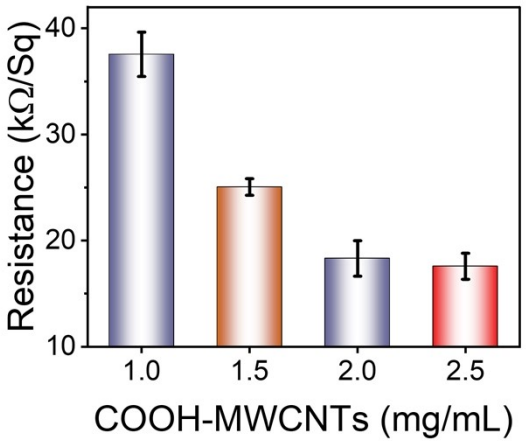

Figure S4. Square resistance parameter of Janus films made with different concentrations of the COOH-MWCNTs dispersion.

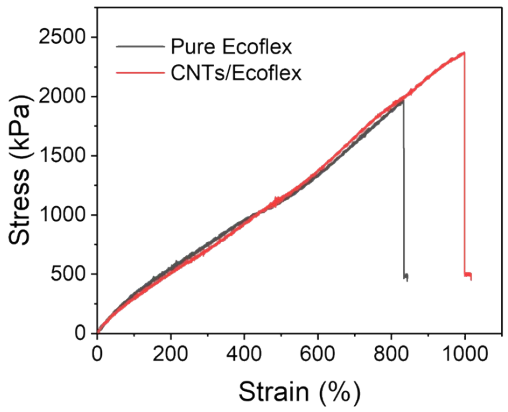

Fig. S5. Stress-strain curves of the pure Ecoflex membrane and CNTs/ Ecoflex Janus film.

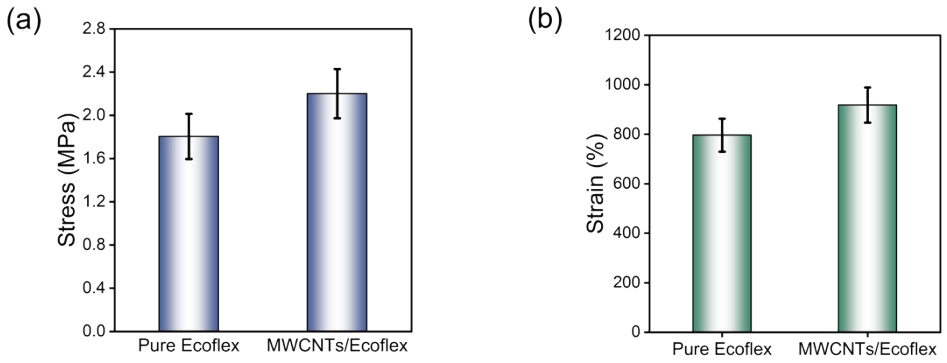

Fig. S6. The mechanical strength of the CNTs/Ecoflex Janus film compared with pure Ecoflex membrane. (a) Breaking strength. (b) Elongation at break.

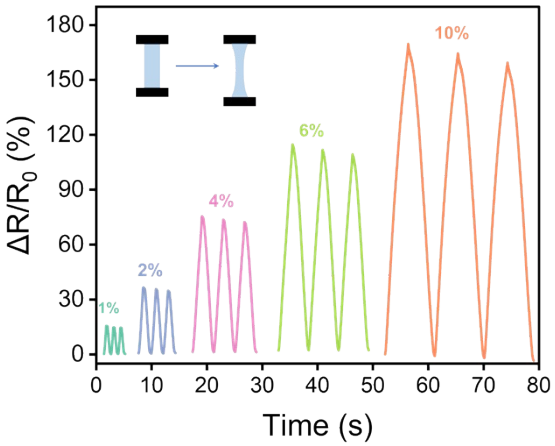

Fig. S7. The normalized resistance versus time curves of the Janus films under different deformations (from 1 to 10%).

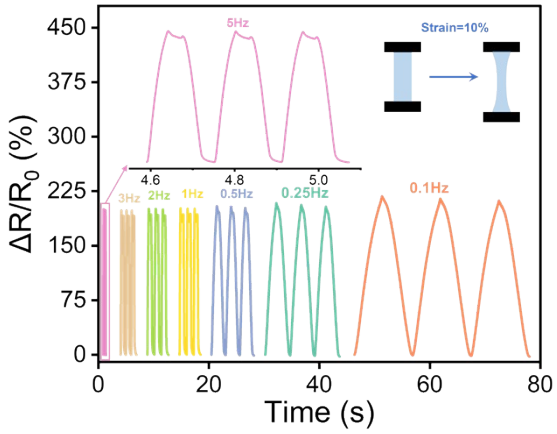

Fig. S8. The normalized resistance versus time curves of the Janus films under different frequencies (from 0.1 to 5 Hz) between 0 and 10% strain.

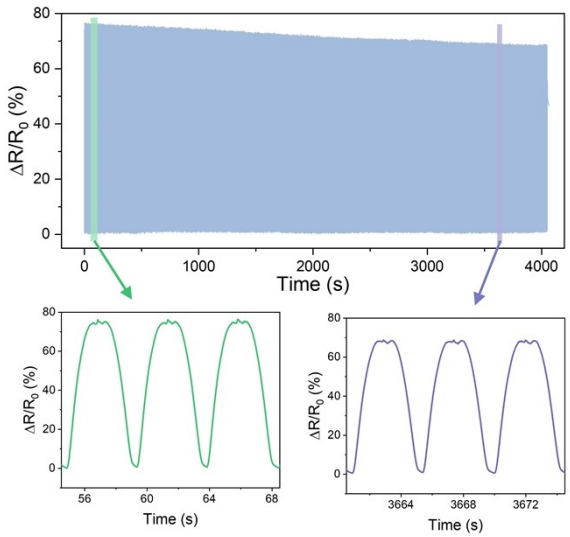

Figure S9. Normalized resistance of Janus film undergoing 2000 cycles of stretching.

Fig. S10. A self-supported Janus films with a diameter of 25 mm expanded under the applied pressure of 0, 4, 8, 12, and 16 kPa, respectively.

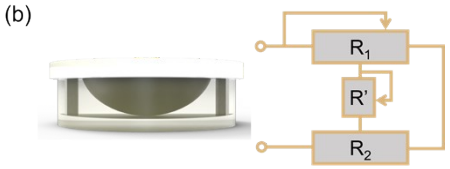

Fig. S11. Circuit diagram of the sensor. (a) Series circuit under small deformation, the self-supported conductive layer is R_1 and the supported conductive layer is R_2. (b) Parallel circuit under large deformation, R' is the new resistance formed by the contact between the conductive films.

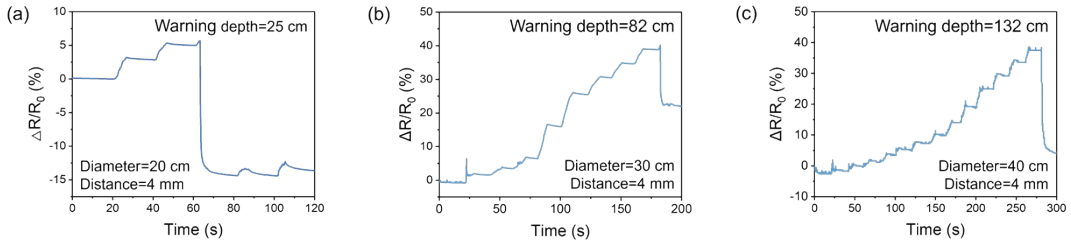

Fig. S12. The normalized resistance versus time curves with depth of descent and corresponding warning depth for sensors (Distance=4 mm, Diameter=20, 30 and 40 mm) respectively in underwater tests.

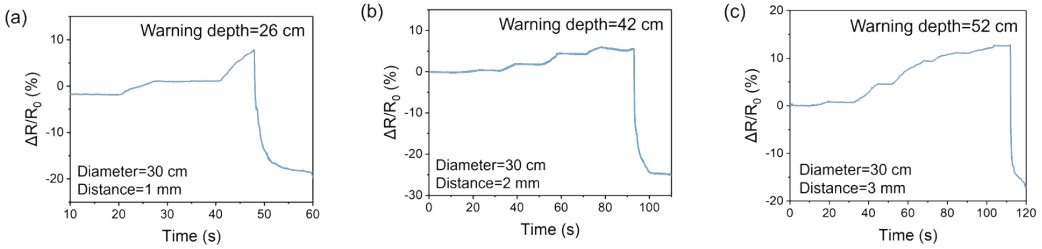

Fig. S13. The normalized resistance versus time curves with depth of descent and corresponding warning depth for sensors (Diameter=30 mm, Distance=1, 2 and 3 mm) respectively in underwater tests.

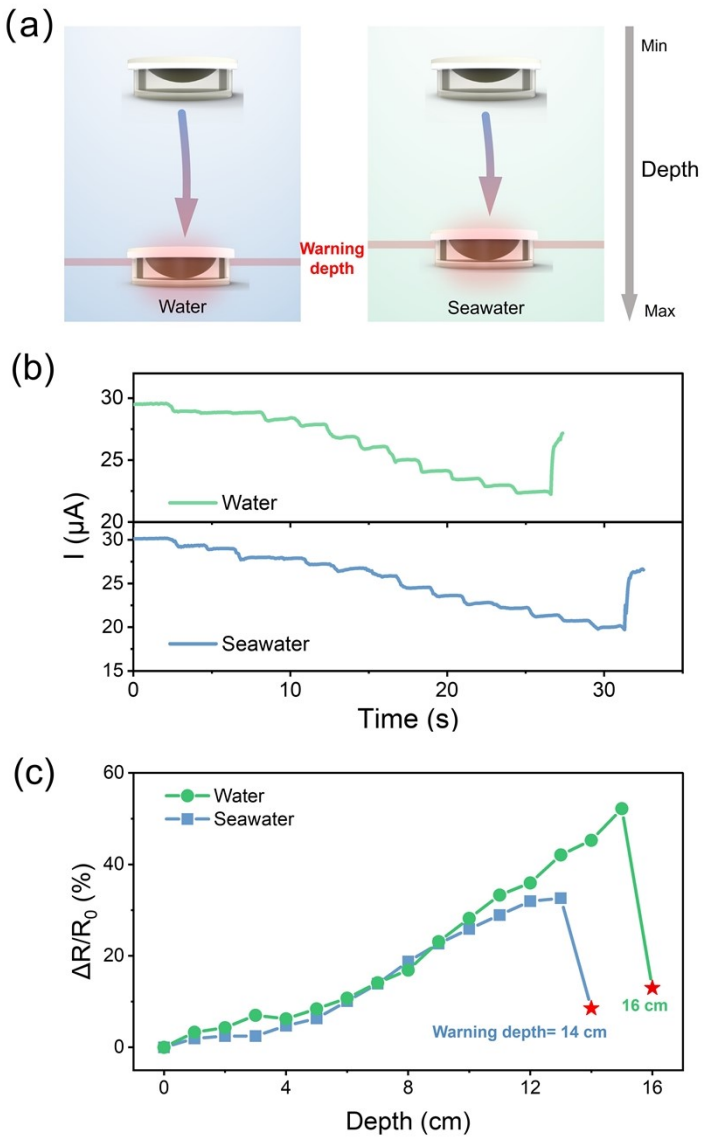

Figure S14. Differences in sensing performance of underwater sensors in seawater and water. （a）Diagram of the experimental process. (b) Real-time variation curve of the current signal of the sensors. (c) Normalised resistance versus depth curve of the sensors.

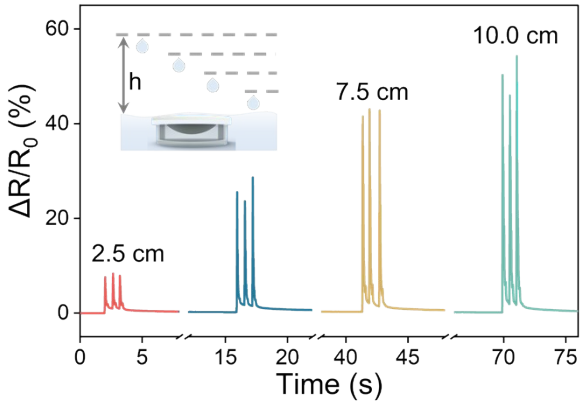

Fig. S15. The normalized resistance versus time curves of the sensors were measured for droplets at a) varying heights (2.5, 5.0, 7.5, and 10 cm) when dropped onto the water surface.

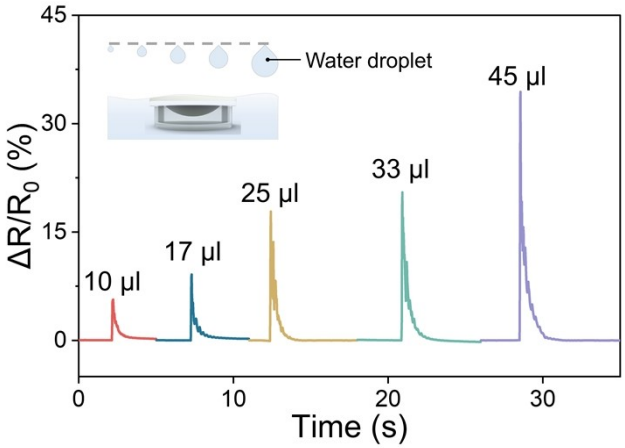

Fig. S16. The normalized resistance versus time curves of the sensors were measured for droplets volumes (10, 16.7, 25, 33.3, and 50 µl) when dropped onto the water surface.

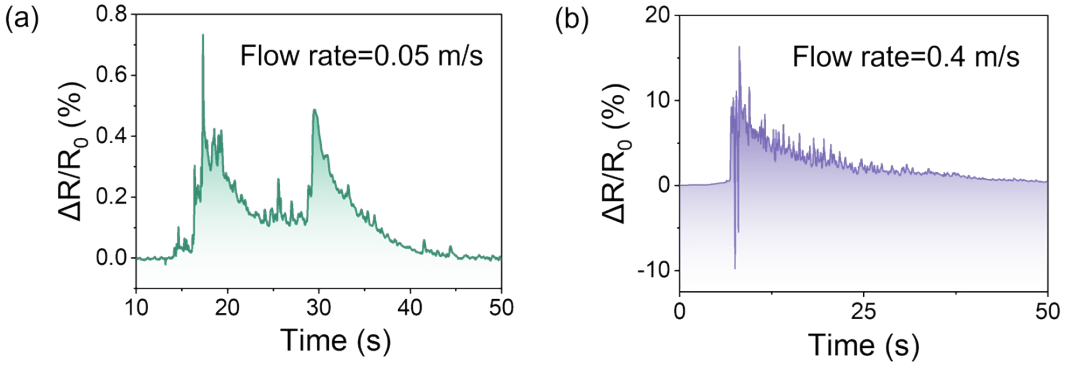

Fig. S17. Amplified detection of the normalized resistance versus time curves at different maximum instantaneous flow rates, (a)flow rate=0.05 m/s, (b) flow rate=0.4 m/s.

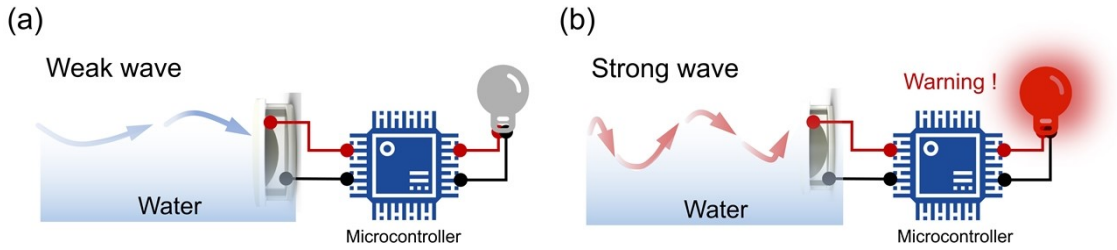

Fig. S18. Schematic diagram of the closed-loop system of the scene consisting of the sensor, microcontroller and LED in (a) weakwave and (b) strong wave state.

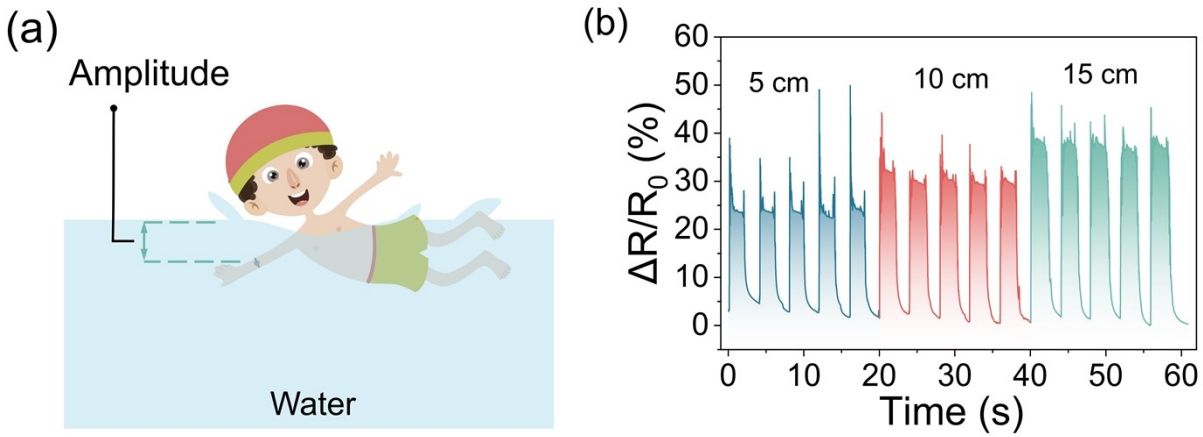

Fig. S19. (a) Diagram of the wearable sensor monitoring the amplitude (5, 10 and 15 cm) of the up and down arm stroked during swimming and (b) the corresponding normalized resistance versus time curves of the sensors.

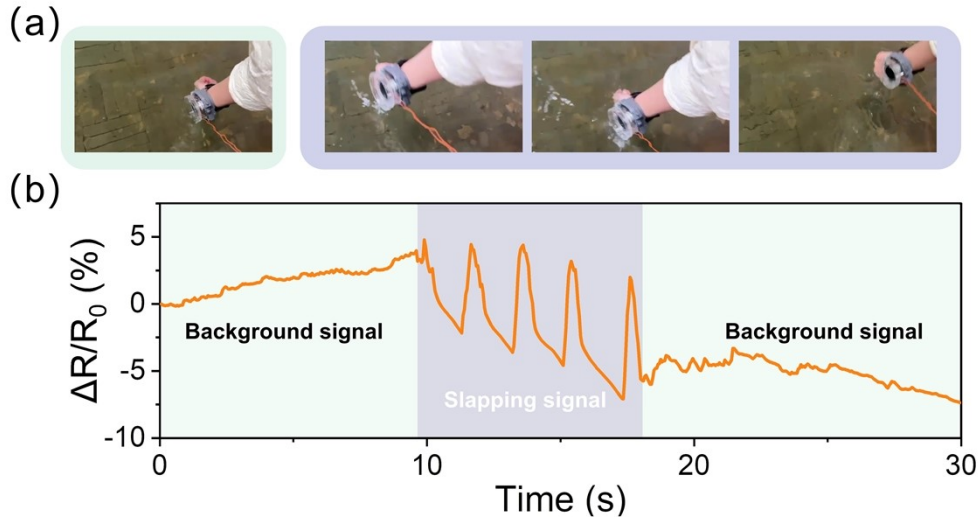

Figure S20. (a) Photos of the volunteer wearing wearable sensors for experiments in outdoor waters. (Outdoor wind speed: 5 m/s) (b) The sensor monitors the motion signal of slapping water against the background signal of outdoor wind disturbances.

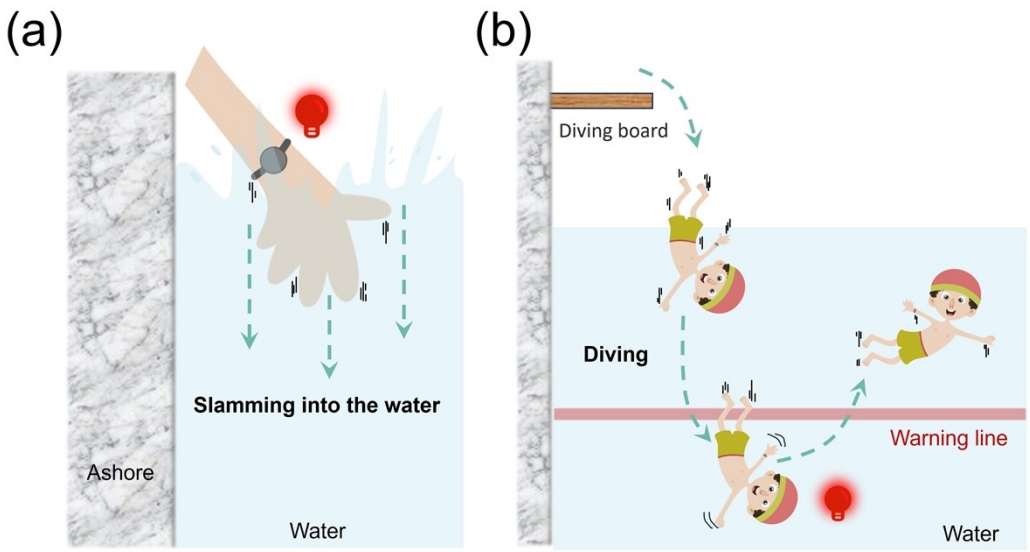

Figure S21. The illustrations on potential failure modes and false alarms of the sensors. (a) The volunteer stond on the ashore and slammed his hand into the water violently to activate the alarm by mistake. (b) False alarm triggered by diving into the water to the warning depth, but the volunteer would float quickly under buoyancy without drowning.